

# RELIABILITY OF FLOATING STRUCTURES: EXTREME RESPONSE AND LOAD FACTOR DESIGN<sup>a</sup>

By Steven R. Winterstein,<sup>1</sup> Alok K. Jha,<sup>2</sup> and Satyendra Kumar<sup>3</sup>

**ABSTRACT:** The reliability of a floating offshore platform against extreme offsets is studied. Methods are illustrated to perform more refined analyses of extreme loads and load effects. These include the effect of nonlinear diffraction under random wave excitation. They permit inclusion of randomness in significant wave height  $H_s$ , in peak spectral period,  $T_p$  given  $H_s$ , and also in the extreme load effect given both  $H_s$  and  $T_p$ . Numerical effects are demonstrated by applying these methods to a specific floating structure: a deep-draft spar buoy. Design of the spar has been considered in two deep-water sites, one in the Gulf of Mexico and another in the Northern North Sea. Appropriate joint contours of significant wave height and peak period are developed, and these are used to develop load and resistance factors for each of the two sites.

## INTRODUCTION

Floating structures are an attractive option to support oil and gas production in deep water. They promise relatively economic designs, with little sensitivity to increases in water depth. Corresponding challenges arise from complex fluid-structure interactions, which lead to basic hydrodynamic questions of estimating applied forces and restoring properties such as damping. The novelty of these structures suggests the need to study their reliability and to consider practical load and resistance factor design (LRFD) procedures for such structures. These would parallel recent LRFD guidelines for fixed structures ("API" 1993).

The writers consider here one specific floating structure: a deep-draft cylinder known as a spar buoy (Fig. 1). This concept has gained considerable industry interest. This paper focuses on a particular spar buoy (Fig. 2), which serves as the "theme structure" of the NSF Center for Offshore Technology Research (OTRC) in Texas. This spar has draft  $h = 198$  m, diameter  $d = 42.7$  m, and a center well to protect drilling and production risers. The writers specifically study its reliability against extreme surge offsets, based on state-of-the-art nonlinear diffraction force models (Kim and Yue 1988). Reliability consequences and necessary load and resistance factors are considered for typical sites in the Gulf of Mexico and in the North Sea.

## Load Factor Design

In load and resistance factor design, nominal loads and resistances are scaled by separate factors,  $\gamma_L$  and  $\phi_R$ , to achieve desired reliability levels. The use of several factors rather than a single multiplier on the net safety margin aims to achieve more uniform reliability over cases where loads show notably more uncertainty than resistances, as well as other cases where they may show comparable variability or even less. Similarly, different factors may be applied to separate load contributions that show different variability. Examples include separate factors for dead and live loads, or the separate factors recently

suggested for static, wave-frequency, and slow-drift loads on floating structures (Banan et al. 1994).

Here, the writers consider the extreme offset of the spar under wave loads only. In this case, the dominant force contribution comes from wave diffraction effects, which cause both a mean drift force and also slowly varying oscillating forces [as can be seen later in the paper; see (6)]. These slowly varying forces are significant, as they drive the resonant dynamic response of a flexibly moored offshore structure such as the spar. In view of the dominance of these slow-drift loads, the writers retain here a single load factor  $\gamma_L$  along with a resistance factor of  $\phi_R$ :

$$\phi_R R_{nom} \geq \gamma_L L_{nom} \quad (1)$$

The nominal wave load level,  $L_{nom}$ , is in turn commonly associated in some way with a return period of 100 years. Various definitions of  $L_{nom}$  may be considered:

- Case 1:  $L_{nom,1} = L(H_{100})$ , the representative load associated with the 100-year significant wave height,  $H_{100}$ , and associated  $T_p$  value. Uncertainty is neglected both in  $T_p$  and in the load given  $H_s$ .

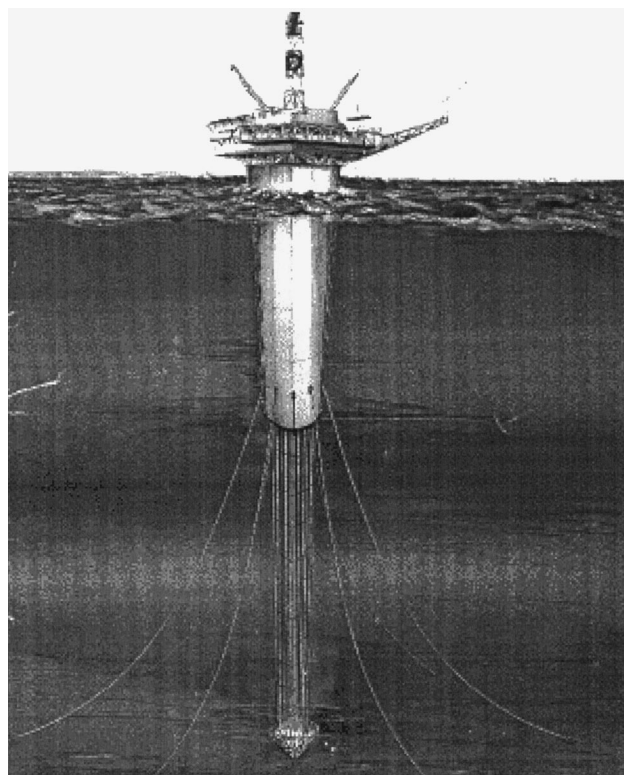


FIG. 1. Spar Buoy Concept

<sup>a</sup>Presented at the May 1–4, 1995, Offshore Technology Conference (OTC), held at Houston, TX.

<sup>1</sup>Civ. and Envir. Engrg. Dept., Stanford Univ., Stanford, CA 94305-4020.

<sup>2</sup>Sr. Engr., Bechtel Offshore, 45 Fremont St., San Francisco, CA 94105-1895.

<sup>3</sup>Software Consultant, Trilogy Software, Austin, TX 78730.

Note. Discussion open until January 1, 2000. To extend the closing date one month, a written request must be filed with the ASCE Manager of Journals. The manuscript for this paper was submitted for review and possible publication on March 21, 1996. This paper is part of the *Journal of Waterway, Port, Coastal, and Ocean Engineering*, Vol. 125, No. 4, July/August, 1999. ©ASCE, ISSN 0733-950X/99/0004-0163-0169/\$8.00 + \$.50 per page. Paper No. 12800.

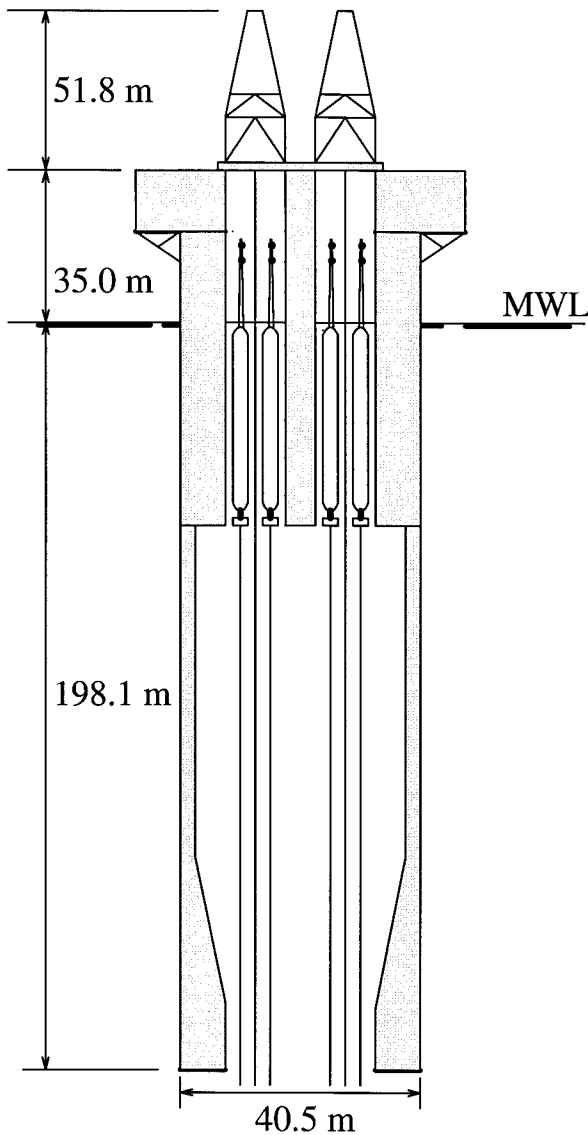


FIG. 2. Spar Elevation

- Case 2:  $L_{nom,2} = L((H_s, T_p)_{100})$ , the 100-year load including randomness in  $H_s$  and  $T_p$ . Uncertainty is neglected only in the load given both  $H_s$  and  $T_p$ .
- Case 3:  $L_{nom,3} = L_{100}$ , the “true” 100-year load. This includes uncertainty in both  $H_s$  and  $T_p$ , as well as in the load given  $H_s$  and  $T_p$ .

It is clear that, by more fully including complete uncertainty, these loads increase in order, i.e.,  $L_{nom,1} \leq L_{nom,2} \leq L_{nom,3}$ . For fixed structures that are most sensitive to wave height, this increase may not be too great. Greater differences may be expected for floating structures, however, due to potential dynamic amplification of wave sub- and superharmonics.

In principle, of course, any choice of nominal load  $L_{nom}$  can be used if associated with a consistent load factor. This would suggest a higher  $\gamma_L$  with  $L_{nom,2}$ , than with  $L_{nom,3}$ , and a still higher  $\gamma_L$  associated with  $L_{nom,1}$ . The main drawback is that the ratio  $L_{nom,3}/L_{nom,1}$  may depend on both the structure and the environment. Because a factor  $\gamma_L$  applied to  $L_{nom,1}$  cannot reflect this dependence, it must lead to a range of reliability levels. The virtue of  $L_{nom,3}$  is that it carries the most case-specific information on both structure and site. Its corresponding drawback is that it is the most difficult to calculate. The writers show here some simple methods to perform these more detailed load calculations and the impact on design load factors for the spar buoy.

## METHODOLOGY

### Wave Environment

Because floating structures can show significant dynamic effects, the wave elevation  $\eta(t)$  at the platform center should be modeled as an irregular, random process with appropriate frequency content. This is most commonly parameterized by the significant wave height,  $H_s = 4\sigma_\eta$ , and the peak spectral period  $T_p$ .

Following common approaches for both North Sea and Gulf of Mexico sites, the writers model only large wave “events” in which  $H_s$  exceeds a specified threshold  $h_{min}$ . In particular, three-hour sea states with  $H_s > h_{min}$  are assumed to follow a truncated Weibull distribution:

$$G_{H_s}(h) = P[H_s > h] = \exp \left[ -\left(\frac{h}{h_0}\right)^\gamma + \left(\frac{h_{min}}{h_0}\right)^\gamma \right] \quad (2)$$

Assuming events with  $H_s > h_{min}$  occur independently with an annual rate  $\nu$ , the distribution of annual maximum  $H_s$  values is

$$F_{ann}(h) = P[\max \text{ annual } H_s \leq h] = \exp[-\nu G_{H_s}(h)] \quad (3)$$

Fig. 3 compares the distribution,  $F_{ann}$ , of the annual maximum in (3) from four site-specific models of  $G_{H_s}(h)$ :

- GOM1: A generic Gulf of Mexico site, subjected to the full hurricane population (Banon et al. 1994). This formed the basis of an industry study on code calibration of tension-leg platforms.
- GOM 2: The combined population of sudden hurricanes and winter storms in the Gulf of Mexico. This has defined nonevacuable events on which American Petroleum Institute requalification standards have been based (Petrauskas et al. 1994).
- NNS: The Statfjord site in the Northern North Sea (Haver and Gudmestad 1992).
- SNS: The Ekofisk site in the Southern North Sea (Haver and Gudmestad 1992).

Table 1 gives parameter values of  $h_{min}$ ,  $\nu$ ,  $h_0$ , and  $\gamma$  in cases GOM1, NNS, and SNS. This table also lists parameters of the conditional distribution of  $T_p$  given  $H_s$ . Because floating structures have already been installed at the GOM1 and NNS sites, these cases will be considered in subsequent spar buoy analyses.

Results for GOM2 have been inferred here numerically from figure 5 of Petrauskas et al. (1994). That figure describes maximum wave heights, which are divided here by

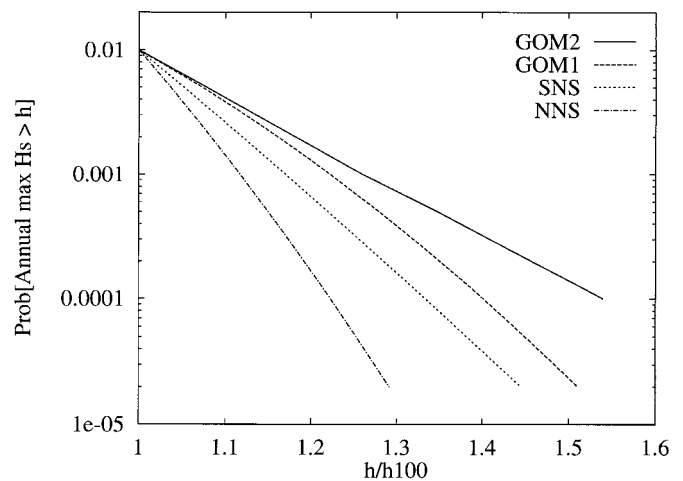


FIG. 3. Annual Significant Wave Height  $H_s$

**TABLE 1. Environmental Parameters**

| Parameter<br>(1)                        | GOM1<br>(2)     | NNS<br>(3)              | SNS<br>(4)             |
|---|-----------------|-------------------------|------------------------|
| Storm threshold $h_{min}$ (m)           | 8.00            | 7.50                    | 6.50                   |
| Expected annual number of storms, $\nu$ | 0.10            | 7.60                    | 5.80                   |
| (a) Significant wave height $H_s$       |                 |                         |                        |
| Scale parameter $h_0$ (m)               | 6.42            | 4.58                    | 2.03                   |
| Shape parameter $\gamma$                | 2.29            | 2.00                    | 1.25                   |
| $H_{100}$ (m)                           | 11.7            | 14.0                    | 13.5                   |
| $H_{1,000}$ (m)                         | 14.3            | 15.6                    | 15.8                   |
| $H_{1,000}/H_{100}$                     | 1.22            | 1.11                    | 1.17                   |
| (b) Spectral peak period $T_p$          |                 |                         |                        |
| Distribution type                       | Normal          | Lognormal               | Lognormal              |
| $E(T_p H_s = h)$ (s)                    | $5.39h^{0.382}$ | $-14.5 + 16.8h^{0.227}$ | $-2.6 + 6.59h^{0.382}$ |
| $COV(T_p H_s)$                          | 0.06            | 0.09                    | 0.09                   |
| Median ( $T_p H_s = H_{100}$ ) (s)      | 13.8            | 16.0                    | 15.1                   |
| Median ( $T_p H_s = H_{1,000}$ ) (s)    | 14.9            | 16.8                    | 16.2                   |

$\sqrt{2} \ln N/2 = 1.86$  to estimate  $H_s$  values in an associated sea state with  $N = 1,000$  cycles. Note that figure 1 of this same reference includes a similar plot of the full hurricane population, which, when rescaled by 1.86, agrees quite well with the GOM1 fit described herein.

Note from Table 1 that the 100-year significant wave height,  $H_{100}$ , is generally larger for the North Sea sites than for the Gulf of Mexico. Conversely, Fig. 3 shows that smaller  $H_{100}$  values are often associated with broader wave height distributions above  $H_{100}$ . For example, the sudden storm population (GOM2) has the smallest  $H_{100}$  value, but its distribution decays most slowly above  $H_{100}$ . Indeed, in Fig. 3, the decay rates of all four distributions vary directly with  $H_{100}$ : the largest  $H_{100}$  case (NNS) decays most quickly; the smallest  $H_{100}$  case (GOM2) decays most slowly; etc.

This suggests that, at least for fixed structures, where the nominal load  $L_{nom,1} = L(H_{100})$  may suffice, larger load factors  $\gamma_L$  may be needed in the Gulf of Mexico to achieve the same reliability as in the North Sea. (A further aspect not considered here is the consequence of failure; lower reliability levels may suffice in the Gulf if evacuation policies can avoid life loss.)

Because floating structures are sensitive to  $T_p$  as well as  $H_s$ , their load factors should be based on joint models of  $H_s$  and  $T_p$ . Such models are shown below for both GOM and NS sites.

**100-Year  $H_s-T_p$  Contours**

The goal here is to find convenient estimates of  $L_{nom,2} = L((H_s, T_p)_{100})$ , the 100-year load including uncertainty in both  $H_s$  and  $T_p$ . For this purpose, it is useful to seek a “100-year  $H_s-T_p$  contour,” which, when searched, yields the 100-year load for any structural load quantity.

Fig. 4 shows several possible 100-year contours for the GOM1 (full hurricane) environment. The simple “100-year pdf” contour is obtained by finding equally likely outcomes (constant pdf), outside which we fall with probability  $p_f = .01$  per year, or  $.01/\nu$  per event. This contour will generally give a conservative estimate of the 100-year load  $L_{nom,2}$ . In fact, the worst load along this 100-year pdf contour will be the 100-year load only if every  $H_s-T_p$  value outside this contour leads to failure. (It is also assumed here that the worst load inside any such  $H_s-T_p$  contour does not exceed the worst load along the contour.) The general conservatism of the 100-year pdf contour is shown by its largest  $H_s$  value, 12.8 m, which exceeds the marginal 100-year value  $H_{100} = 11.7$  m that applies for wave-height dominated structures.

In contrast, Fig. 4 also shows a new contour definition based on concepts of the inverse FORM method (Winterstein et al. 1993). Physically, it assumes that the failure region does not include all possible  $H_s-T_p$  values outside the contour, but

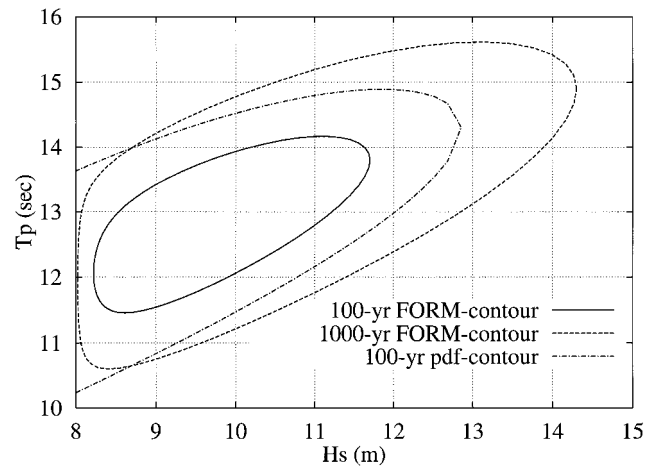


**FIG. 4.  $H_s-T_p$  Contour**

rather any possible straight line that is tangent to the contour. One such tangent is the vertical line  $H_s = H_{100}$ ; thus, the 100-year FORM contour includes the traditional value  $H_s = H_{100} = 11.7$  m (with representative  $T_p$ ) as a special case. (As a technicality, to simplify the probability calculations, these contours are generated first in terms of independent, standard normal variables  $U_1$  and  $U_2$ , and then transformed to physical variables  $H_s$  and  $T_p$ .) Note that FORM estimates of rare-probability events are supported by both theory and numerous applications. Therefore, the writers believe this 100-year FORM contour provides a useful tool for extreme load estimation, increasingly accurate as the return period increases. In contrast, note from Fig. 4 that the 100-year pdf contour falls roughly equidistant between the 100- and 1,000-year FORM contours.

**Wave Load and Response Model**

The method used to predict the hydrodynamic loading on a structural member generally depends on both wave and structural parameters. For members whose dimensions in the along-wave direction are small compared with the wave length, it is common to assume that the fluid flow is unaffected by the presence of the structure. In this case, wave radiation and diffraction are commonly ignored, and the loading is estimated by the Morison equation. For floating structures, however, the dimensions of their hulls suggest that wave radiation and diffraction must be included. Thus, the diffraction theory is used here to model the wave loads on the spar buoy. [Note that the diffraction load model used here has been systematically studied and compared with wave tank experiments for the spar buoy under consideration here; cf. Jha et al. (1997). Good agreement has been found for both North Sea and Gulf of Mexico sea states. Viscous effects are found to be relatively less important, and their primary effect is to induce additional damping. This is modeled here through an assumed linear viscous damping coefficient, taken here to be 5% of critical damping, in view of the experimental results.]

The use of linear diffraction theory to predict wave loads is well established, and various numerical radiation-diffraction codes for these linear (first-order) loads are available. Specifically, assume that the irregular, random wave elevation  $\eta(t)$  is given by the following Fourier representation:

$$\eta(t) = \sum_{k=1}^N A_k \cos(\omega_k t + \theta_k) = \text{Re} \sum_{k=1}^N C_k \exp[i(\omega_k t)] \quad (4)$$

in terms of the wave frequency  $\omega_k$ , phase  $\theta_k$ , and associated (complex) Fourier amplitude  $C_k = A_k \exp(i\theta_k)$ . In this case, the resulting first-order surge force  $f_1(t)$  can be similarly expressed as

$$f_1(t) = \text{Re} \sum_{k=1}^N C_k H_f(\omega_k) \exp[i(\omega_k t)] \quad (5)$$

In this result, the first-order diffraction analysis provides  $H_f(\omega_k)$ , the (complex-valued) “transfer function” between a wave (with frequency  $\omega_k$ ) and the corresponding first-order load at the frequency.

To include nonlinear effects in the frequency-domain diffraction problem, a common approach is to consider the linear result as the first term in a perturbation expansion. For the irregular wave elevation  $\eta(t)$  given above, the corresponding second-order contribution,  $f_2(t)$ , can be expressed as follows:

$$f_2(t) = \text{Re} \sum_{k=1}^N \sum_{l=1}^N C_k C_l H_{ff}(\omega_k, \omega_l) \exp\{i[(\omega_k - \omega_l)t]\} \quad (6)$$

Thus, the second-order perturbation gives rise to force contributions at all possible differences ( $\omega_k - \omega_l$ ) between pairs of incident wave frequencies  $\omega_k$  and  $\omega_l$ . Here  $H_{ff}(\omega_k, \omega_l)$  is referred to as a quadratic transfer function (QTF), which is the result produced by a second-order diffraction analysis. [There is also a load contribution at the sum frequency ( $\omega_k + \omega_l$ ), but this is omitted here, as only the slowly varying, difference-frequency loads cause resonant responses with the flexible mooring system of the spar.]

The offshore industry has devoted considerable resources to the development and verification of second-order diffraction codes (e.g., WAMIT 1995). Estimation of the quadratic transfer function for each frequency pair of interest is generally an expensive calculation. The writers perform this here with a specific second-order load calculation algorithm, which is especially efficient for axisymmetric bodies such as the spar (Kim and Yue 1988).

The response of interest here is  $X_{\max}$ , the maximum of the surge offset  $x(t)$  in a three-hour sea state. Statistics of  $X_{\max}$  are found from the postprocessing analysis routine TFPOP (Ude 1994). This uses the first- and second-order load transfer functions,  $H_f(\omega_k)$  and  $H_{ff}(\omega_k, \omega_l)$ , as well as the added mass and damping from (first-order) wave radiation. TFPOP then constructs corresponding first- and second-order transfer functions to response  $x(t)$ . (In general, it can include forces/moments in all six degrees of freedom and analyze any response quantity, such as motion, acceleration, tether tension, etc.) A convenient model of nonlinear random vibration, the “Hermite” model, is then used to predict various fractiles of  $X_{\max}$ . This model has been verified through simulation for both TLPs and semisubmersible platforms (Winterstein et al. 1994) and for the spar buoy (Winterstein et al. 1995).

## RESULTS

Figs. 5 and 6 apply the foregoing methodology to study the extreme surge offset in the full hurricane (GOM1) environment. Fig. 5 shows  $H_s-T_p$  contours for this site with return periods of  $10^2$ ,  $10^3$ , and  $10^4$  years. Also shown are lines along which the median extreme offset (in a three-hour sea state) is constant. These have been created by the TFPOP routine, assuming a JONSWAP wave spectrum with  $\gamma = 3.3$ .

The results show, for example, that a sea state with a 100-year  $H_s = H_{100} = 11.7$  m and associated  $T_p = 13.8$  s gives an offset slightly above 14 m. This is the load effect previously denoted  $L_{\text{nom},1}$ , the 100-year result that reflects variability in  $H_s$  only. To also include the effect of random  $T_p$ , the writers select the maximum offset along the 100-year  $H_s-T_p$  contour. This value, denoted  $L_{\text{nom},2}$  is nearly 16 m. It is caused by a sea state with a less-than-100 year  $H_s$  in a relatively steep sea state (a smaller-than-average  $T_p$ ) for which nonlinear effects are large. This shows the importance of considering the entire  $H_s-T_p$  contour for floating structure response. Similar results can be

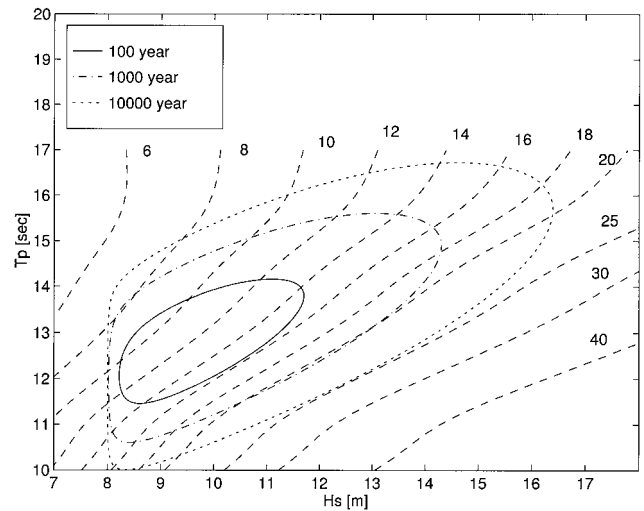


FIG. 5. Surge Offset Isolines (GOM1)

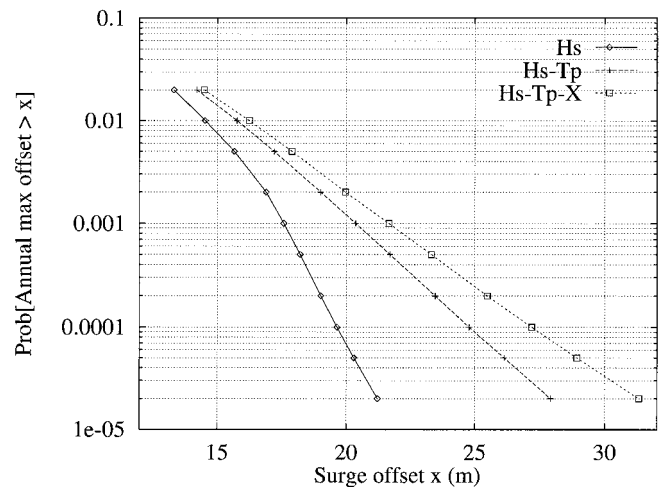


FIG. 6. Extreme Surge Offset (GOM1)

obtained for different return periods, through contours with appropriate return periods (e.g., 1,000 or 10,000 year).

Fig. 6 shows such results versus the annual failure probability,  $p_f$ . Here, the labels  $H_s$  and  $H_s-T_p$  refer to those quantities considered random; thus,  $H_s$  and  $H_s-T_p$  correspond to  $L_{\text{nom},1}$  and  $L_{\text{nom},2}$ . The final  $L_{\text{nom},3}$ , the actual 100-year load effect, is labeled  $H_s-T_p-X$ , because it includes uncertainty in maximum response  $X$  as well as in  $H_s$  and  $T_p$ . This last result is still largest; here,  $L_{100}$  is a bit above 16 m. It is found by inflating the contours in Fig. 5 to account for the additional randomness in  $X_{\max}$  (Winterstein et al. 1995).

Note that randomness in  $X_{\max}$  causes the 100-year load effect to grow and higher load fractiles to grow still more. Thus, it leads to a slower decay of the load distribution (case  $H_s-T_p-X$  versus others in Fig. 6). For subsequent load factor calculations, note the numerical value  $L_{1,000}/L_{100} = 1.33$ , found from the  $H_s-T_p-X$  curve in Fig. 6.

Fig. 7 shows results analogous to Fig. 5 for the NNS site. Compared with the GOM1 result, the NNS model is shown to give not only larger  $H_s$  values, but also broader conditional distributions of  $T_p$  given  $H_s$ . These relatively steeper sea states might be expected to give significantly greater slow-drift motions. Indeed, this effect would be particularly notable if the unimodal JONSWAP spectral model is retained. (To see this, combine the isoresponse lines from Fig. 5 with the environmental contours of Fig. 7.) However, the writers have also modified the isoresponse lines in Fig. 7, by using a two-peaked

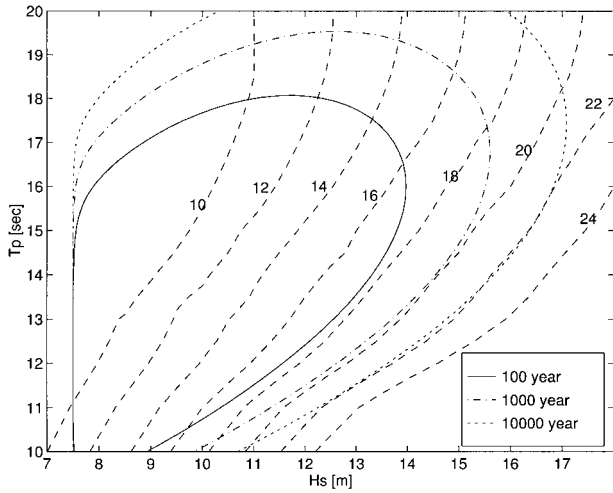


FIG. 7. Surge Offset Isolines (NNS)

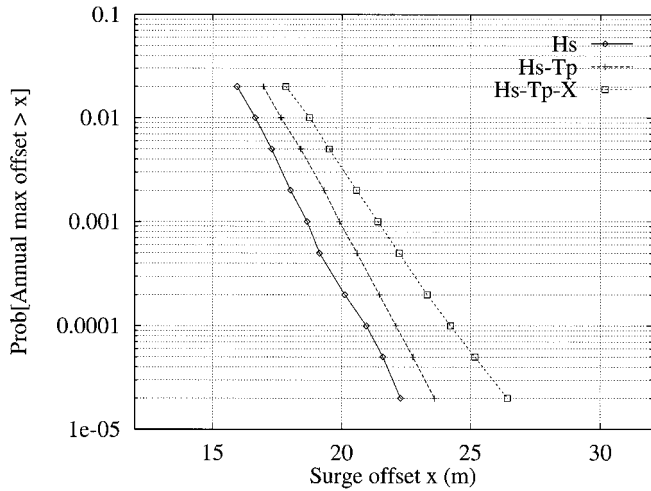


FIG. 8. Extreme Surge Offset (NNS)

wave spectral model suggested by Torsethaugen in this range (Bitner-Gregersen and Haver 1991).

Fig. 8 shows the resulting distribution of extreme offset in the NNS, analogous to Fig. 6 for the same spar located at the GOM1 site. Now the ratio  $L_{1,000}/L_{100} = 1.16$ , compared with  $L_{1,000}/L_{100} = 1.33$  for the GOM1 case. Thus, the distribution of load effect is predicted to decay roughly twice as quickly in the NNS as in the GOM1. It is shown below that this directly impacts the relative load factors needed for the two sites. The writers caution here, however, that such results hinge on the modeling assumptions made herein—that is, the  $H_s-T_p$  joint distribution, the associated wave spectrum, and finally, the resulting slow-drift forces in relatively steep, small- $T_p$  sea states. Additional study of these modeling issues would appear useful.

## LOAD AND RESISTANCE FACTORS

Finally, the writers show the effect of including uncertainty in the resistance,  $R$ , of the spar against surge motions. Here, the writers use its median  $\hat{R}$  as the nominal resistance and the 100-year applied offset,  $L_{100}$ , as the nominal load effect. The writers then use an LRFD checking equation as in (1):

$$\phi_R \hat{R} \geq \gamma_L L_{100} \quad (7)$$

Thus, the writers seek load and resistance factors,  $\gamma_L$  and  $\phi_R$ , that give a desired survival probability,  $1 - p_f$ , and associated reliability index  $\beta = \Phi^{-1}(1 - p_f)$ .

The FORM method is again convenient in this context. For

a given design, it estimates not only  $p_f = P[R < L]$ , but also the most likely resistance and load,  $R^*$  and  $L^*$ , to produce failure. While this most-likely FORM result generally requires numerical optimization, closed-form results are available if  $R$  and  $L$  are assumed independent and lognormal:

$$R^* = \hat{R} \exp(-\sigma_{\ln R} \alpha_R \beta); \quad L^* = \hat{L} \exp(\sigma_{\ln L} \alpha_L \beta) \quad (8)$$

in which  $\hat{L}$  = median load value; and the  $\alpha$  factors = relative “importance” factors (uncertainty contributions) to the total safety margin  $\ln R - \ln L$ :

$$\alpha_R = \frac{\sigma_{\ln R}}{[\sigma_{\ln R}^2 + \sigma_{\ln L}^2]^{0.5}}; \quad \alpha_L = \frac{\sigma_{\ln L}}{[\sigma_{\ln R}^2 + \sigma_{\ln L}^2]^{0.5}} \quad (9)$$

Finally, from (7) we set  $R^* = \phi_R \hat{R}$  and  $L^* = \gamma_L L_{100}$  and from (8) we find the resulting factors

$$\phi_R = \exp(-\sigma_{\ln R} \alpha_R \beta); \quad \gamma_L = \frac{\hat{L}}{L_{100}} \exp(\sigma_{\ln L} \alpha_L \beta) \quad (10)$$

These results form the basis of LRFD guidelines for fixed offshore structures (“Recommended” 1993). As noted in its Commentary C, the factor  $\hat{L}/L_{100}$  is sometimes denoted a “bias factor”  $B$ , which reflects the fractile of the nominal load.

Eq. (10) may be used directly if the lognormal model is appropriate over the entire range of loads and resistances. This may not be true in general; for example, the annual maximum surge load effect appears to fall off roughly exponentially in Fig. 6. The lognormal load model may still be useful if it is appropriately tail-fit, however, to model the important load values that contribute significantly to failure. Here, the writers fit to  $L_{100}$  and  $L_{1,000}$ , given respectively by  $\hat{L} \exp(2.32\sigma_{\ln L})$  and  $\hat{L} \exp(3.09\sigma_{\ln L})$  for a lognormal model of  $L$ . It is then possible to express the lognormal distribution parameters,  $\hat{L}$  and  $\sigma_{\ln L}$ , in terms of  $L_{100}$  and  $L_{1,000}$ . Substituting these into (10), we find a simple result for the load factor  $\gamma_L$ :

$$\gamma_L = \left( \frac{L_{1,000}}{L_{100}} \right)^{1.3(\alpha_L \beta - 2.32)} \quad (11)$$

For example, consider the case where there is no resistance variability ( $\sigma_{\ln R} = 0$ ), and the annual failure probability  $p_f = 10^{-3}$  is sought. In this case,  $\alpha_L = 1$  and  $\beta = 3.09$ , so that (11) reduces simply to  $\gamma_L = L_{1,000}/L_{100}$ . This is natural, because if the resistance is fixed, the load factor  $\gamma_L$  must entirely cover the increase in target return period (here, from the 100-year nominal to the 1,000-year target level). More generally, as the resistance variability  $\sigma_{\ln R}$  grows, the load factor  $\gamma_L$  will decrease, due to reduction in  $\alpha_L$ . This is because, as resistance variability increases, the 1,000-year safety margin is more likely caused by a less-than-1,000 year load, together with an appropriate lower fractile of the resistance.

Fig. 9 shows the results of applying (10)–(11) for the GOM1 site. Results are shown for different values of the resistance coefficient of variation,  $V_R$ , and thus of  $\sigma_{\ln R}^2 = \ln(1 + V_R^2)$ . For  $V_R = \sigma_{\ln R} = 0$ , a target  $p_f = 10^{-3}$  is achieved with  $\phi_R = 1$  and  $\gamma_L = L_{1,000}/L_{100}$ , or 1.33 from Fig. 6. If we increase  $\sigma_{\ln R}$  to 0.1, Fig. 9 shows the most likely failure scenario to be covered by a somewhat reduced load factor of  $\gamma_L = 1.28$ , together with a resistance factor  $\phi_R = .92$  to reflect the growing chance of less-than-average resistances.

Finally, Fig. 10 shows analogous load and resistance factors for the NNS site. Because it has a narrower distribution of extreme loads (Fig. 8 versus Fig. 6), this site requires lower load factors for the same target  $p_f$ . Equivalently, the same load factor in spar buoy design will lead to higher reliability in the NNS site than in the Gulf of Mexico. Returning, for example, to the  $\sigma_{\ln R} = 0$  case, a load factor  $\gamma_L = 1.31$  can achieve annual  $p_f = 10^{-4}$  in NNS, while only about  $10^{-3}$  in the GOM1 site.

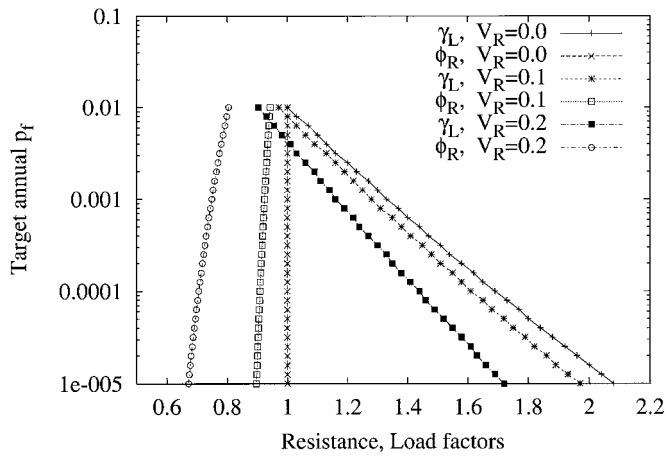


FIG. 9. Load and Resistance Factors (GOM1)

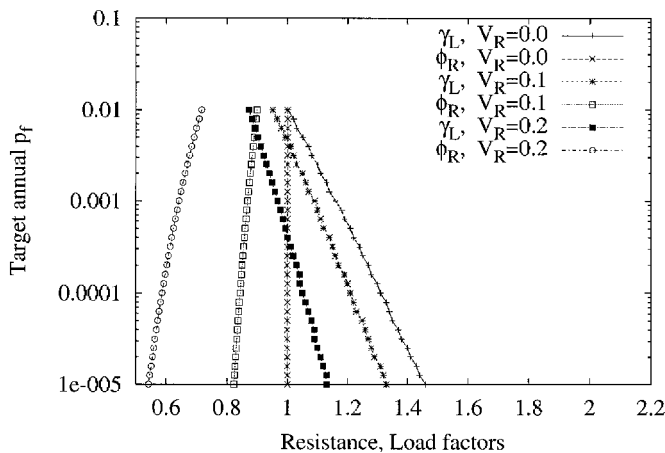


FIG. 10. Load and Resistance Factors (NNS)

(The difference in consequence—e.g., potential worker hazards in NNS if evacuation is not feasible—may make these disparate safety levels reasonable. If so, it may happen that similar load factors are appropriate, although merely by the happenstance of offsetting effects. This choice of appropriate  $p_f$  requires further study, however.) Also, because the load distribution is narrower in the NNS, the same resistance variability plays a larger relative role in determining reliability. Thus, Fig. 10 shows that the resulting resistance factor  $\phi_R$  should be set more conservatively (lower) in the NNS than in the GOM1 site.

## SUMMARY AND CONCLUSIONS

The reliability of a floating offshore platform against extreme offsets has been studied. Two main aspects have been considered. First, methods have been illustrated to perform more refined analysis of extreme slow-drift loads and load effects. Results were shown for the 100-year significant wave height, for the 100-year ocean environment, and finally for the 100-year load. Second, these methods have been applied to a specific floating structure: a deep-draft spar buoy. Design of the spar has been considered in both Gulf of Mexico and North Sea sites, and appropriate load and resistance factors have been illustrated for each site. The results shown below apply to this specific spar buoy and at the specific sites chosen.

Numerical results have included the following:

- The 100-year  $H_s$  value,  $H_{100}$ , is found to be generally lower in the Gulf of Mexico cases considered here than in the North Sea sites (Table 1). Above  $H_{100}$ , however, the distribution of  $H_s$  falls off more quickly in the North Sea

(Fig. 3). For example,  $H_{1,000}/H_{100}$  is 1.11 in the Northern North Sea (NNS) site, while ranging in the Gulf of Mexico from 1.22 (case GOM1; all hurricanes) to 1.26 (case GOM2: sudden hurricanes and winter storms). This is notable, because nominal loads are generally based on 100-year conditions, and load factors must then account for the difference between this nominal-load return period and a longer target life (e.g.,  $10^3$ – $10^4$  years).

- Diffraction analysis predicts that extreme surge offsets of the spar buoy are dominated by second-order effects, with forces proportional to  $H_s^2$ . In this, they are somewhat similar to drag-dominated jackets, whose base shear forces also grow roughly with  $H_s^2$ . Compared with jackets, however, floating structure extremes show greater sensitivity to spectral peak period  $T_p$  (Figs. 5 and 7). These figures show that the 100-year load,  $L_{100}$ , is most likely caused with less-than-100 year  $H_s$ , which combines with a less-than-average  $T_p$  to give a relatively steep sea state, in which nonlinear effects are greatest.
- By searching 100- and 1,000-year contours of  $H_s$ – $T_p$ , load levels such as  $L_{100}$  and  $L_{1,000}$  can be estimated. Results for the spar again vary notably across sites:  $L_{1,000}/L_{100}$  is estimated to be 1.33 in the GOM1 site, while only 1.16 in the NNS (Figs. 6 and 8).
- The dominant effect of steep, small- $T_p$  sea states implies an associated modeling burden. It suggests a need to reassess the accuracy of our environmental models, of both the long-term  $H_s$ – $T_p$  scattergram in this region and the associated wave spectrum, in these sea states. While the NNS contours seem to sample a wider range of steep sea states, the consequence of extreme surge levels is reduced notably by replacing a unimodal JONSWAP spectrum with a bimodal (Bitner-Gregersen and Haver 1991). (Compare isoresponse lines in Figs. 5 and 7. The structural model is the same; their sole source of difference is the assumption of unimodal versus bimodal wave spectrum.)

Future work will consider more general load and resistance factor calibration, over a suite of sites and spar buoy designs. The writers will also seek to include load modeling uncertainty, analogous to the empirical uncertainty assigned to the drag coefficient  $C_D$  for Morison forces on fixed platforms. Modeling uncertainty associated with nonlinear diffraction can be viewed as causing an analogous “ $C_M$  uncertainty.” This uncertainty may usefully be split into errors in first- and second-order load effects, the latter expected to be greater due to modeling errors in both second-order loads and associated damping. These studies will require systematic comparison of observed versus predicted loads or load effects—and observations will include the suite of spar buoy tests recently performed in the Offshore Technology Research Center wave tank at Texas A&M.

## ACKNOWLEDGMENTS

This study was supported by the Offshore Technology Research Center, National Science Foundation Engineering Research Centers Program Grant Number CDR-8721512. Additional support has been supplied by the Reliability of Marine Structures (RMS) program of Stanford University.

## APPENDIX. REFERENCES

- Banon, H., Toro, G. R., Jefferys, E. R., De, R. S. (1994). “Development of reliability-based global design equations for TLPs.” *Proc., 13th Int. Offshore Mech. Artic Engrg. Symp.*, American Society of Mechanical Engineers, New York, 2, 335–343.
- Bitner-Gregersen, E., and Haver, S. (1991). “Joint environmental model for reliability calculations.” *Proc., 1st Int. Offshore Polar Engrg. Conf.*,

- International Society of Offshore and Polar Engineers, Golden, Colo, 472–478.
- Haver, S., and Gudmestad, O. (1992). “Uncertainties related to the kinematics of ocean waves and their effect on structural reliability.” *Proc., 2nd Int. Offshore Polar Engrg. Conf.*, International Society of Offshore and Polar Engineers, Golden, Colo., 472–478.
- Jha, A. K., de Jong, P. R., and Winterstein, S. R. (1997). “Motions of a spar buoy in random seas: comparing predictions and model test results.” *Proc., BOSS-97*, 2, Delft Univ., 333–347.
- Kim, M. H., and Yue, D. K. P. (1988). “The nonlinear sum-frequency wave excitation and response of a tension-leg platform.” *Proc., BOSS’88*, Trondheim, Norway.
- Petrauskas, C., Finnigan, T. D., Heideman, J. C., Vogel, M., Santala, M., and Berek, G. P. (1994). “Metocean criteria/loads for use in assessment of existing offshore platforms.” *Proc., Offshore Technol. Conf.*, Offshore Technology Conference, Houston, Tex., 3, 155–167.
- “Recommended practice for planning, designing and constructing fixed offshore platforms—load and resistance factor design.” (1993). *API RP2A-LRFD*, American Petroleum Institute, Washington, D.C.
- Ude, T.C. (1994). “TFPOP: a program for analyzing second-order load and response models of offshore structures.” *Rep. RMS-15*, Reliability of Marine Struct. Program, Stanford University, Stanford, Calif.
- WAMIT: a radiation-diffraction panel program for wave-body interactions—user’s manual.* (1995). Dept. of Oc. Engrg., Massachusetts Institute of Technology, Cambridge, Mass.
- Winterstein, S. R., Kumar, S., and Kleiven, G. (1995). “Environmental contours and extreme response of deep-water floating structures.” *Proc., 10th Engrg. Mech. Specialty Conf.*, ASCE, Reston, Va., 2, 1187–1190.
- Winterstein, S. R., Ude, T. C., Cornell, C. A., Bjerager, P., and Haver, S. (1993). “Environmental parameters for extreme response: inverse FORM with omission factors.” *Proc., ICOSAR-93*, Balkema, Rotterdam, The Netherlands.
- Winterstein, S. R., Ude, T. C., and Kleiven, G. (1994). “Springing and slow-drift responses: predicted extremes and fatigue vs. simulation.” *Proc., BOSS-94*, Massachusetts Institute of Technology, Cambridge, Mass., 3, 1–15.